
POLYCONVEX PHYSICS-AUGMENTED NEURAL NETWORK CONSTITUTIVE MODELS IN PRINCIPAL STRETCHES

A PREPRINT

Adrian Buganza Tepole
Columbia University
New York City, NY, USA

Asgar Jadoon
The University of Texas at Austin
Austin TX, USA

Manuel Rausch
The University of Texas at Austin
Austin TX, USA

Jan N. Fuhg
The University of Texas at Austin
Austin TX, USA

ABSTRACT

Accurate constitutive models of soft materials are crucial for understanding their mechanical behavior and ensuring reliable predictions in the design process. To this end, scientific machine learning research has produced flexible and general material model architectures that can capture the behavior of a wide range of materials, reducing the need for expert-constructed closed-form models. The focus has gradually shifted towards embedding physical constraints in the network architecture to regularize these over-parameterized models. Two popular approaches are input convex neural networks (ICNN) and neural ordinary differential equations (NODE). A related alternative has been the generalization of closed-form models, such as sparse regression from a large library. Remarkably, all prior work using ICNN or NODE uses the invariants of the Cauchy-Green tensor and none uses the principal stretches. In this work, we construct general polyconvex functions of the principal stretches in a physics-aware deep-learning framework and offer insights and comparisons to invariant-based formulations. The framework is based on recent developments to characterize polyconvex functions in terms of convex functions of the right stretch tensor \mathbf{U} , its cofactor $\text{cof}\mathbf{U}$, and its determinant J . Any convex function of a symmetric second-order tensor can be described with a convex and symmetric function of its eigenvalues. Thus, we first describe convex functions of \mathbf{U} and $\text{cof}\mathbf{U}$ in terms of their respective eigenvalues using deep Holder sets composed with ICNN functions. A third ICNN takes as input J and the two convex functions of \mathbf{U} and $\text{cof}\mathbf{U}$, and returns the strain energy as output. The ability of the model to capture arbitrary materials is demonstrated using synthetic and experimental data.

1 Introduction

Constitutive models of soft materials are essential for selecting the appropriate material and designing structures undergoing extreme deformations. Accurate material models are also key to our understanding of the physiology and disease of soft tissue. Scientific machine learning research has produced flexible and general material model architectures that are able to capture a wide range of materials, reducing the need for expert-constructed closed-form models [1, 2, 3]. Initial efforts in this area attempted to directly learn strain-stress data pairs using fully connected neural networks [4, 5, 6, 7]. However, the focus has gradually shifted towards embedding physics constraints in the architecture such that these are satisfied by default [2, 8]. Three popular approaches are input convex neural networks (ICNN) [9, 10], neural ordinary differential equations (NODE) [11, 12], and generalizations of closed form models such as sparse regression from a large library or constitutive artificial neural networks [13, 14]. To comply with objectivity and in the case of isotropic materials, strain energy functions in terms of the isotropic invariants of the right Cauchy Green deformation tensor, \mathbf{C} , or its eigenvalues (the squares of the principal stretches) are used [15]. Remarkably, most if not all of the data-driven approaches with ICNN or NODE are based on the invariants of \mathbf{C} [2]. Data-driven models based on sparse regression or model discovery out of a library of existing models have

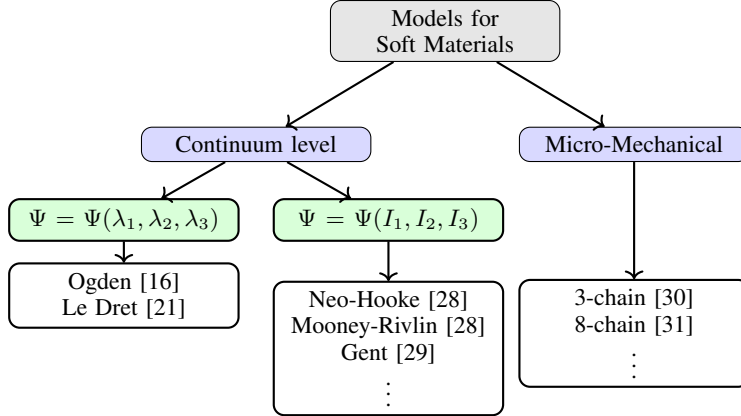


Figure 1: Classification of standard constitutive models for soft materials

occasionally incorporated the Ogden model [16], which is the only constitutive equation in terms of the squares of the principal stretches [17]. The Ogden model has been highly successful in capturing the mechanical response of rubbers and biological tissues with a very simple form [18, 19]. However, surprisingly, there are barely any other examples of constitutive models in terms of principal stretches (Fig. 1) [20]. An extension of the original Ogden model including a similar polynomial expansion for $\text{cof}\mathbf{C}$ was introduced in [21, 22]. To our knowledge, no further developments have been attempted since [20].

In this manuscript, we were interested in building general polyconvex functions of the principal stretches in a physics-aware deep-learning framework, beyond the Ogden model. Our formulation relies on recent characterization of polyconvex functions in terms of convex functions of the right stretch tensor, $\mathbf{U} = \sqrt{\mathbf{C}}$, its cofactor $\text{cof}\mathbf{U}$, and its determinant J [23, 24]. Any convex function of a symmetric second-order tensor can be described with a convex and symmetric function of its eigenvalues [25]. To build convex functions of \mathbf{U} and $\text{cof}\mathbf{U}$ in terms of their respective eigenvalues, we rely on a class of permutation invariant neural networks known as deep Holder sets [26, 27]. A composition of deep Holder sets with ICNNs can be used to describe general symmetric convex functions. With these building blocks, we can capture general polyconvex functions in terms of the principal stretches.

2 Polyconvex strain energies in terms of principal stretches

Hyperelastic materials are described by a scalar strain energy potential, $\Psi(\mathbf{F})$, as a function of the deformation gradient, \mathbf{F} . This potential cannot be entirely arbitrary but rather must conform to physically meaningful constraints. The most important considerations for Ψ are material symmetries, objectivity, and exhibiting some form of convexity. Ball showed that polyconvexity of Ψ is sufficient to guarantee the existence of solutions to boundary value problems where the material is hyperelastic (existence of global minimizers) [32]. While this requirement is not necessary and on occasions, it might be too restrictive [33], it is convenient because it is a local condition on the strain energy as opposed to the necessary condition of quasi-convexity [32]. Polyconvexity requires Ψ to be a convex function on the extended set of arguments including \mathbf{F} , but also its cofactor and determinant,

$$\tilde{\Psi}(\mathbf{F}, \text{cof}\mathbf{F}, \det \mathbf{F}) \quad (1)$$

In other words, $\tilde{\Psi}$ is convex in \mathbb{R}^{19} ($\mathbf{F}, \text{cof}\mathbf{F} \in \mathbb{R}^3 \times \mathbb{R}^3$ and $J = \det \mathbf{F} \in \mathbb{R}$).

Explicit dependence on the deformation gradient is usually avoided because \mathbf{F} is not objective. Instead, to guarantee objectivity *a priori*, Ψ (or rather $\tilde{\Psi}$) is assumed a function of the right Cauchy Green deformation tensor $\mathbf{C} = \mathbf{F}^T \mathbf{F}$. Additionally, consideration of material symmetries restricts the functional dependence of $\Psi(\mathbf{C})$. For example, for isotropic materials, the invariants $I_1 = \text{tr}\mathbf{C}$, $I_2 = \text{cof}\mathbf{C}$, $I_3 = \det\mathbf{C} = J^2$ are used. Polyconvexity of invariant based models of the form $\tilde{\Psi}(\mathbf{C}, \text{cof}\mathbf{C}, J)$, or more precisely $\tilde{\Psi}(I_1, I_2, J)$ requires that $\tilde{\Psi}$ is convex non-decreasing with respect to I_1, I_2 and convex with respect to J . Note that this is because I_1 is quadratic in \mathbf{F} while I_2 is quadratic in $\text{cof}\mathbf{F}$. Therefore, composition with convex non-decreasing functions is needed to retain convexity with respect to \mathbf{F} and $\text{cof}\mathbf{F}$ [34].

Alternatively, the eigenvalues of \mathbf{C} , which are the squared of the principal stretches, λ_i^2 , are also invariant under rotation and therefore can be used as arguments of an isotropic strain energy potential [35]. However, models in terms of principal stretches are rare. The most common constitutive model in terms of principal stretches is the Ogden model [20, 18]. Only recently have there been other efforts to propose strain energies in terms of λ_i^2 [36]. Yet, even recent attempts to formulate Ψ in terms of principal stretches are not general enough; they only depend on isotropic functions of λ_i^2 and thus only consider convexity with respect to \mathbf{F} and not $\text{cof}\mathbf{F}$ [36, 17]. Furthermore, the square of the principal stretches λ_i^2 or even powers $\lambda_i^{2\alpha}$ lead to convex functions of \mathbf{C} and not necessarily with respect to \mathbf{F} . Steigmann showed a general description of polyconvex energies in terms of the stretch tensor stemming from the polar decomposition of the deformation gradient [23],

$$\mathbf{F} = \mathbf{R}\mathbf{U} \quad , \quad (2)$$

with

$$\mathbf{U} = \sum_i \lambda_i \mathbf{n}_i \otimes \mathbf{n}_i \quad . \quad (3)$$

Steigmann showed that polyconvexity of Ψ can be achieved by constructing a special class of polyconvex functions of \mathbf{U}

$$\tilde{\Psi}(\mathbf{F}, \text{cof}\mathbf{F}, \det\{(\mathbf{F})\}) = \tilde{\Psi}(\mathbf{U}, \text{cof}\mathbf{U}, \det\mathbf{U}) \quad , \quad (4)$$

convex on the extended domain $[\mathbf{U}, \text{cof}\mathbf{U}, \det\mathbf{U}]$. However, the potentials explored by Steigmann were in terms of the invariants $i_1 = \text{tr}\mathbf{U}$, $i_2 = \text{tr}(\text{cof}\mathbf{U})$ [23]. Namely, the potentials were of the form

$$\tilde{\Psi}(i_1, i_2, J) \quad (5)$$

convex on the three arguments. The result has been recently extended to more general functions of the principal stretches λ_i by Wiedemann and Peter [24]. Considering again Eq. (4), $\tilde{\Psi}$ has to be convex in $[\mathbf{U}, \text{cof}\mathbf{U}, \det\mathbf{U}]$. Consider first a convex function $g(\mathbf{U})$. There exists a function $\tilde{g}(\boldsymbol{\lambda}) = g(\mathbf{U})$ such that $\tilde{g}(\bullet)$ is convex and symmetric on its arguments, with $\boldsymbol{\lambda} \in \mathbb{R}^d$ is the vector of eigenvalues of \mathbf{U} for dimensions $d = 2, 3$ [37, 25]. In our case, we consider 3-dimensional elasticity such that $\tilde{g}(\lambda_1, \lambda_2, \lambda_3)$ is a convex and symmetric function, i.e. invariant under permutations of the arguments.

Similarly, consider the cofactor $\text{cof}\mathbf{U}$, we have the expansion in terms of the principal stretches

$$\begin{aligned} \text{cof}\mathbf{U} &= \det\{(\mathbf{U})\}\mathbf{U}^{-T} = (\lambda_1\lambda_2\lambda_3) \left(\sum_i \frac{1}{\lambda_i} \mathbf{n}_i \otimes \mathbf{n}_i \right) \\ &= \lambda_2\lambda_3 \mathbf{n}_1 \otimes \mathbf{n}_1 + \lambda_1\lambda_3 \mathbf{n}_2 \otimes \mathbf{n}_2 + \lambda_1\lambda_2 \mathbf{n}_3 \otimes \mathbf{n}_3 . \end{aligned} \quad (6)$$

Then, for a convex function of $\text{cof}\mathbf{U}$ we need a convex function $\tilde{h}(\lambda_1\lambda_2, \lambda_1\lambda_3, \lambda_2\lambda_3)$ convex and symmetric on its three arguments, the eigenvalues of $\text{cof}\mathbf{U}$.

Thus, a polyconvex material can be expressed as [24]

$$\tilde{\Psi}(\lambda_1, \lambda_2, \lambda_3, \lambda_1\lambda_2, \lambda_1\lambda_3, \lambda_2\lambda_3, J) \quad (7)$$

convex on its arguments, and invariant under permutations of $\lambda_1, \lambda_2, \lambda_3$ and also invariant under permutations of $\lambda_1\lambda_2, \lambda_1\lambda_3, \lambda_2\lambda_3$.

3 Existing Hyperelastic Potentials in Terms of Principal Stretches

As mentioned before, there are very few examples of strain energies in terms of the principal stretches. Undoubtedly the most well-known is the one proposed by Ogden [16], which has remained one of the most accurate for modeling rubber mechanics [19] and has also proven useful in other domains such as modeling of soft tissue [18]. The incompressible Ogden model is

$$\Psi_{\text{O}} = \sum_1^p \frac{2\mu_p}{\alpha_p^2} (\lambda_1^{\alpha_p} + \lambda_2^{\alpha_p} + \lambda_3^{\alpha_p} - 3) - p(J - 1) . \quad (8)$$

Type	Deformation	Relevant experimental output
Uniaxial tension (UT) 	$\mathbf{F} = \begin{bmatrix} \lambda & 0 & 0 \\ 0 & \frac{1}{\sqrt{\lambda}} & 0 \\ 0 & 0 & \frac{1}{\sqrt{\lambda}} \end{bmatrix}$	$\sigma_1 = -\lambda_2 \frac{\partial \Psi}{\partial \lambda_2} + \lambda_1 \frac{\partial \Psi}{\partial \lambda_1}$
Equibiaxial tension (ET) 	$\mathbf{F} = \begin{bmatrix} \lambda & 0 & 0 \\ 0 & \lambda & 0 \\ 0 & 0 & \frac{1}{\lambda^2} \end{bmatrix}$	$\sigma_1 = \sigma_2 = -\lambda_3 \frac{\partial \Psi}{\partial \lambda_3} + \lambda_1 \frac{\partial \Psi}{\partial \lambda_1}$
Pure shear stress (PS) 	$\mathbf{F} = \begin{bmatrix} \lambda & 0 & 0 \\ 0 & 1 & 0 \\ 0 & 0 & \frac{1}{\lambda} \end{bmatrix}$	$\begin{aligned} \sigma_1 &= -\lambda_3 \frac{\partial \Psi}{\partial \lambda_3} + \lambda_1 \frac{\partial \Psi}{\partial \lambda_1} \\ \sigma_2 &= -\lambda_3 \frac{\partial \Psi}{\partial \lambda_3} + \lambda_2 \frac{\partial \Psi}{\partial \lambda_2} \end{aligned}$

Table 1: Studied deformation modes with relevant output

An example of a compressible Ogden model is

$$\Psi_{\text{Oc}}(\lambda_1, \lambda_2, \lambda_3) = \sum_{i=1}^m \frac{\gamma_i}{\alpha_i} (\bar{\lambda}_1^{\alpha_i} + \bar{\lambda}_2^{\alpha_i} + \bar{\lambda}_3^{\alpha_i} - 3) + \kappa \beta^{-2} (\beta \log J + J^{-\beta} - 1) \quad (9)$$

with $\bar{\lambda}_i = J^{-1/3} \lambda_i$. This strain energy is polyconvex for $\gamma_i \alpha_i > 0$, $|\alpha_i| > 1$, $\kappa > 0$, and $\beta > 0$ [38]. We also consider, for completeness, an invariant-based model of a similar polynomial expansion as in Eq. (9). This invariant-based model, commonly known as a generalized Ogden material, takes the form

$$\Psi_{\text{Oi}} = \sum_{i=1}^m c_{i0} (\bar{I}_1 - 3)^i + \sum_{j=1}^n c_{0j} (\bar{I}_2^{3/2} - 3\sqrt{3})^j + \kappa (J^2 + J^{-2} - 2) \quad (10)$$

where $\bar{I}_1 = \text{tr}(J^{-2/3} \mathbf{C})$, $\bar{I}_2 = \text{tr adj}(J^{-2/3} \mathbf{C})$ and polyconvexity requires $c_{i0} \geq 0$, $c_{0j} \geq 0$, $\kappa \geq 0$ [38]. Principal stresses follow [28],

$$\sigma_a = -p + \lambda_a \frac{\partial \Psi_{\text{dev}}}{\partial \lambda_a} \quad (11)$$

where Ψ_{dev} is the deviatoric part of the strain energy, and p can be obtained from either a volumetric strain energy $p = \partial \Psi_{\text{vol}} / \partial J$, for compressible materials, or from boundary conditions in the case of incompressible behavior $J = 1$. Rubber is usually treated as incompressible, thus we present the analytical expressions for the principal stresses in common loading modes considering this assumption. For uniaxial tension, equibiaxial tension, and pure shear the nonzero stresses are summarized in Table 1. For more general loading cases the pressure needs to be determined by imposing $J = 1$ through the corresponding traction boundary conditions. For compressible materials, the pressure is a function of the volumetric strain energy, $p = \partial \Psi_{\text{vol}} / \partial J$. In that case, there is no constraint $J = 1$ and, rather, the unknowns solved from boundary conditions are the transverse stretches. For uniaxial tension, we can define

$$\begin{aligned} \lambda_1 = \lambda, \lambda_2 = \lambda_3 = \lambda_t, \quad \text{with the constraint } \sigma_{22} = \sigma_{33} = 0, \\ \text{and we therefore obtain } \rightarrow \sigma_{22} = 0 = -p(\lambda, \lambda_t) + \frac{1}{\lambda_t} \frac{\partial \Psi}{\partial \lambda_t}, \end{aligned} \quad (12)$$

which needs to be solved for λ_t given λ . Unfortunately, the Eq. (12) is often nonlinear and needs to be solved iteratively, e.g., using Newton-Raphson approaches. For equibiaxial tension, the nonlinear equation to solve becomes with $\lambda_1 = \lambda_2 = \lambda$ and $\sigma_{33} = 0$

$$0 = -p(\lambda, \lambda_3) + \frac{1}{\lambda_3} \frac{\partial \Psi}{\partial \lambda_3}, \quad (13)$$

where the unknown is λ_3 . Lastly, for pure shear, i.e., $\lambda_1 = \lambda, \lambda_2 = 1$ with the constraint $\sigma_{33} = 0$, the equation to solve also takes the form of Eq. (13).

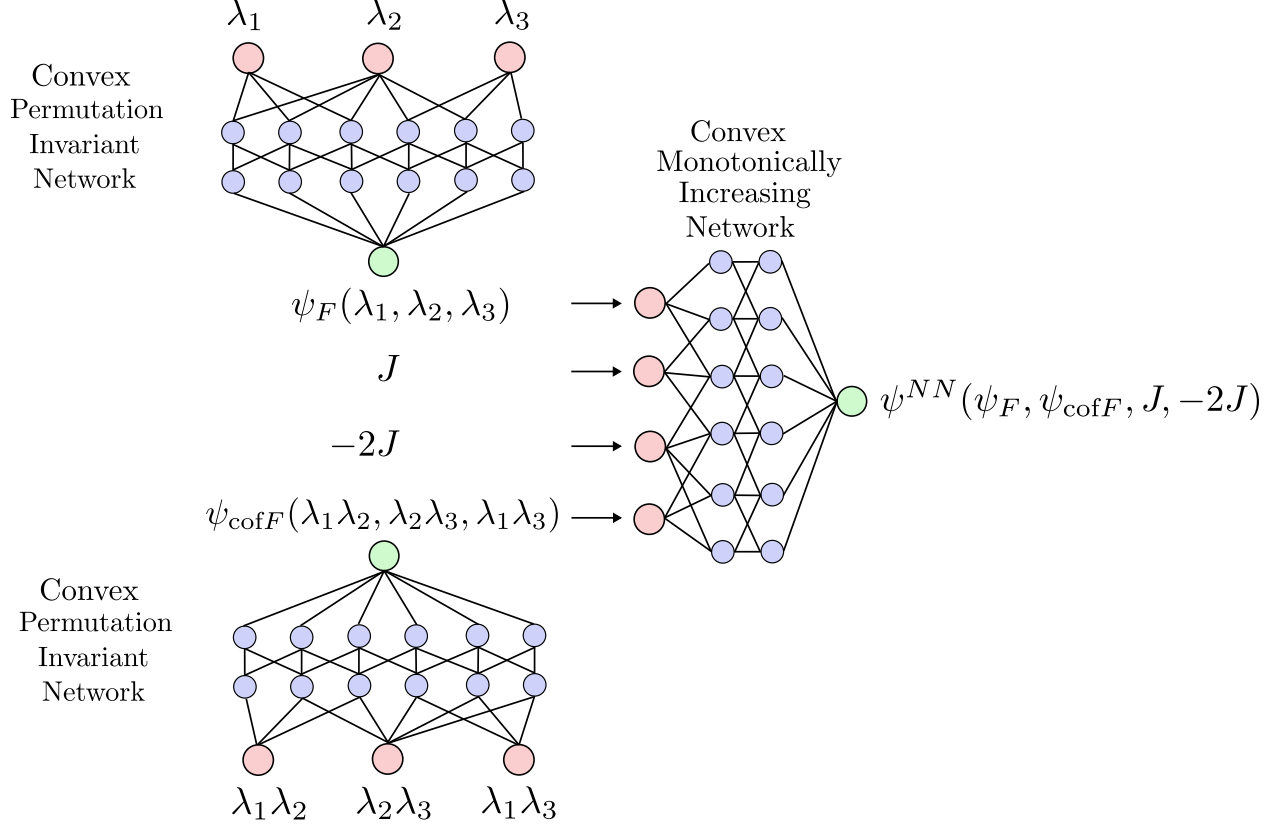


Figure 2: Schematic representation of the presented polyconvex physics-augmented neural network model with principal stretch inputs, λ -PANN.

4 Data-driven Formulation

Following the general polyconvex requirement Eq. (7), we propose the neural network-based model illustrated in Fig. 2,

$$\begin{aligned} \psi &= \psi^{\text{NN}}(\lambda_1, \lambda_2, \lambda_3, \lambda_1\lambda_2, \lambda_2\lambda_3, \lambda_1\lambda_3, \lambda_1\lambda_2\lambda_3, -2\lambda_1\lambda_2\lambda_3) - \psi^{\text{NN}}(1, 1, 1, 1, 1, 1, 1, -2) \\ &\quad - \sum_i o_i(\lambda_i - 1) + \psi^{\text{growth}}(J) \end{aligned} \quad (14)$$

Note that the use of J and $-2J$ is needed to be able to obtain negative stress responses [39]. Since $-2J$ is convex in J , polyconvexity is preserved. We furthermore subtract the constants o_a to guarantee zero stresses in the undeformed state. Also, consider the growth condition

$$\psi^{\text{growth}}(J) = \epsilon \left(\frac{1}{J} + J^2 \right), \quad (15)$$

where we choose $\epsilon = 0.01$ and the general expression of stress

$$\sigma_a = \frac{1}{J} \lambda_a \frac{\partial \psi}{\partial \lambda_a} = \frac{\lambda_a}{J} \left(\frac{\partial \psi^{\text{NN}}}{\partial \lambda_a} - o_a + \frac{\partial \psi^{\text{growth}}}{\partial \lambda_a} \right). \quad (16)$$

Given the desired normalization of the stress $\sigma(\mathbf{F} = \mathbf{I}) = \mathbf{0}$ we obtain

$$\begin{aligned} \sigma_a(\mathbf{F} = \mathbf{I}) = 0 &= \left(\frac{\partial \psi^{\text{NN}}}{\partial \lambda_a} \Big|_{\mathbf{F}=\mathbf{I}} - o_a + \frac{\partial \psi^{\text{growth}}}{\partial \lambda_a} \Big|_{\mathbf{F}=\mathbf{I}} \right) \\ \rightarrow o_a &= \frac{\partial \psi^{\text{NN}}}{\partial \lambda_a} \Big|_{\mathbf{F}=\mathbf{I}} + \frac{\partial \psi^{\text{growth}}}{\partial \lambda_a} \Big|_{\mathbf{F}=\mathbf{I}}. \end{aligned} \quad (17)$$

To satisfy the convexity of ψ^{NN} and also the desired permutation invariances, we split ψ^{NN} into three neural networks as seen in Fig. 2. Two initial neural networks are denoted Ψ_F and $\Psi_{\text{cof}F}$ and produce, as the notation suggests, convex functions of \mathbf{U} and $\text{cof}\mathbf{U}$ by having a permutation invariant function of the eigenvalues $\lambda_1, \lambda_2, \lambda_3$ and $\lambda_1\lambda_2, \lambda_1\lambda_3, \lambda_2\lambda_3$, respectively.

For the permutation invariant neural network we adopt the framework by Kimura et al., which is an extension of the Deep Set framework by Zaheer et al [26, 27]. The Hölder’s Power Deep Sets take the form

$$g(x_1, x_2, x_3) = \rho \left(\left[\sum_i \phi(x_i)^p \right]^{1/p} \right), \quad (18)$$

where ϕ is an input convex neural network, which thus represents a convex function of x_i . Note that the p -norm type approach gives general permutation invariant functions depending on p . For $p = 1$ we get just the mean $(\phi(x_1) + \phi(x_2) + \phi(x_3))/3$ while for $p = \infty$ you get the maximum function $\max(\phi(x_1), \phi(x_2), \phi(x_3))$, which are two common symmetric functions. The function ρ is a convex monotonically increasing function of one scalar argument. The monotonicity constraint is needed to maintain convexity with respect to x_i [34].

After evaluating $\Psi_F, \Psi_{\text{cof}F}$, we pass these outputs through an ICNN to obtain convex non-decreasing functions of \mathbf{U} and $\text{cof}\mathbf{U}$. In addition to taking Ψ_F and $\Psi_{\text{cof}F}$ as inputs, this last ICNN also takes in J and $-2J$ to capture arbitrary convex functions of J . Thus, the λ -PANN architecture in Fig. 2 describes a broad space of polyconvex functions in terms of principal stretches.

5 Results

We first test whether the data-driven formulation is able to capture synthetic Ogden models based on the strain energy Eq. (9). We randomly sampled parameters for Eq. (9) and reported them in Table 2. The parameters are sampled from the following uniform distributions $\beta \sim \mathcal{U}(1, 2)$, $\mu \sim \mathcal{U}(-5, 5)$ and $\alpha \sim \mathcal{U}([-5, -1] \cup [1, 5])$ and the sign of the μ_i, α_i pairs matched to ensure the polyconvex conditions $\mu_i\alpha_i > 0$, $|\alpha_i| > 1$, $\kappa > 0$, and $\beta > 0$.

Table 2: Ogden parameters

μ_1	μ_2	μ_3	α_1	α_2	α_3	κ	β
-2.933	0.101	2.832	-1.019	3.711	2.08	47.592	1.963
0.621	-1.396	0.775	4.878	-3.244	1.075	53.929	1.241
1.786	-2.949	1.163	1.263	-1.174	2.581	37.179	1.206
3.62	-2.375	-1.244	1.268	-1.29	-1.796	17.555	1.109
-0.866	0.375	0.491	-1.672	3.934	2.634	13.146	1.938
1.827	-2.39	0.563	2.061	-1.537	2.208	15.135	1.325
0.294	0.963	-1.258	2.62	1.593	-3.729	12.592	1.652
-1.544	2.315	-0.771	-2.943	1.548	-2.374	22.143	1.307
-0.195	-2.232	2.427	-3.508	-1.861	1.604	27.666	1.109
-0.052	-2.509	2.561	-1.535	-1.568	1.874	22.642	1.256

To generate the data we then randomly sample deformation gradients \mathbf{F} . To fill a broad deformation space we do rejection sampling in the space of deformation gradients,

$$F_{ij} \in \begin{cases} 1 + \mathcal{U}(-\delta, \delta), & \text{if } i = j \\ \mathcal{U}(-\delta, \delta), & \text{else,} \end{cases} \quad (19)$$

where a sample is accepted if

$$-4i_1^3i_3 + i_1^2i_2^2 + 18i_1i_2i_3 - 4i_2^3 - 27i_3^2 \geq 0, \quad (20)$$

with

$$i_1 = \lambda_1 + \lambda_2 + \lambda_3, \quad i_2 = \lambda_1\lambda_2 + \lambda_1\lambda_3 + \lambda_2\lambda_3 \quad i_3 = \lambda_1\lambda_2\lambda_3. \quad (21)$$

The latter is to ensure that the deformation is physical, i.e., $J > 0$ and all principal stretches positive [40]. We generate 200 points for training with $\delta = 0.2$ and 500 points for testing with $\delta = 0.3$. After sampling the deformation gradient,

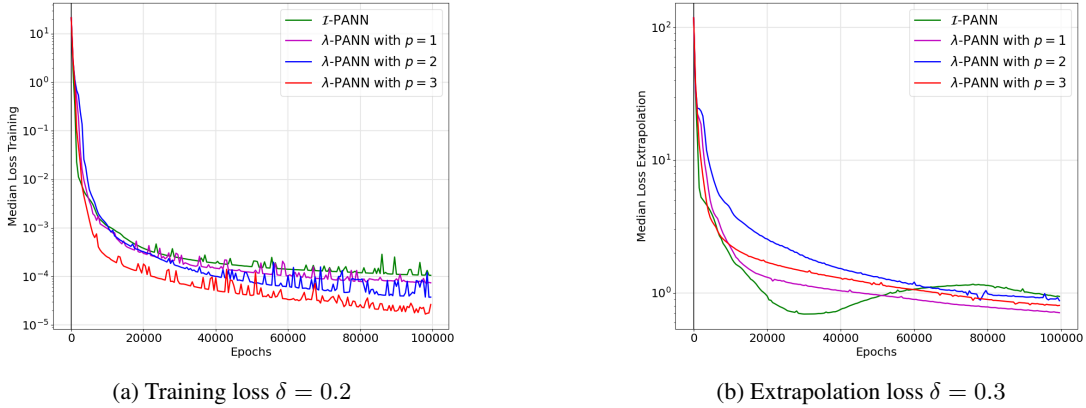


Figure 3: Ogden model median losses over 10 random models as specified in Table 2. a) Training loss; b) Extrapolation loss.

we evaluate the strain energy and stresses according to Eqs. (9). This allows us to build datasets for training and testing

$$\mathcal{D} = \{\mathbf{F}_i, \boldsymbol{\sigma}_i\}_{i=1}^N. \quad (22)$$

Each of the three networks that make up the λ -PANN architecture uses two layers with 10 neurons and a Softplus activation function. This results in 1285 parameters. We utilize the Adam optimizer [41] with a learning rate of 10^{-3} . The median training performances of the proposed data-driven architectures (λ -PANN) across all 10 sampled Ogden models Eq. (9), with parameters in Table 2, are depicted in Fig. 8a. We tested the effect of the power p in the p -norm-like expression at the core of the permutation invariant neural network, the Hölder’s power deep sets Eq. (18). Over 100k epochs, the training loss sharply drops and stabilizes at a minimum, indicating good convergence to an accurate fit with losses $\sim 10^{-4}$. The best performance is achieved with the higher exponent $p = 3$. For comparison, Fig. 8a also shows the training loss of our (and others’) previously developed invariant-based polyconvex neural network (\mathcal{I} -PANN) [39, 42]. To be consistent with the λ -PANN architecture we choose two layers with 23 neurons in the \mathcal{I} -PANN with a Softplus activation function. This results in 1243 parameters and therefore around the same as used for the λ -PANN. We use the same learning rate as before.

While the \mathcal{I} -PANN performs well in the training set, the losses are higher compared to the λ -PANN model. Interestingly, tested on an extrapolation dataset (deformations beyond the training region), the architecture based on principal stretches, λ -PANN, performs better than the invariant-based architecture, \mathcal{I} -PANN. Specifically, the invariant approach, \mathcal{I} -PANN, shows signs of over-fitting: the extrapolation loss first decays but then rises as training progresses (Fig. 3b).

Fig. 4 shows the evaluation of the trained λ -PANN model corresponding to the Ogden material Dataset 5 in Table 2. Results for the two hyper-parameter values, $p = 1$ and $p = 3$, are shown, together with the ground truth evaluation. Even though from Fig. 3, the higher exponent in the permutation invariant neural network, $p = 3$, leads to better than the case $p = 1$, visualizing the results in terms of stress-strain responses under deformations within and outside the training region in Fig. 8b, both models accurately describe the true Ogden model from Dataset 5 with no apparent difference between the two.

We next investigated if the principal stretch data-driven model would perform equally well in a synthetic dataset generated with an invariant model. We used the generalized Ogden model in Eq. (10) and generated stress-strain data by first randomly sampling material parameters reported in Table 3. We uniformly sample the number of active terms to be either two or three, i.e., $m \sim \mathcal{U}_D(2, 3)$ and $n \sim \mathcal{U}_D(2, 3)$ where \mathcal{U}_D is the discrete uniform distributions. We then sample the coefficient values with $c_{i0} \sim \mathcal{U}(0.1, 3.0)$ and $c_{0j} \sim \mathcal{U}(0.1, 3.0)$ as well as $\kappa \sim \mathcal{U}(0.1, 1.0)$. We used the same deformation gradients for training and testing sampled with Eq. (21) for the λ -Ogden dataset. All other (hyper)parameters, such as the number of parameters of the two networks and the learning rate, were also left unchanged.

We trained again the same λ -PANNs as before, with this new dataset. That is, we kept the same architecture (two layers with 10 neurons for each of the networks), and the three p -norm exponents ($p = 1, 2, 3$), and trained for 100k epochs (Fig. 5a). For comparison, we also trained the invariant-based data-driven model \mathcal{I} -PANN [43, 39, 44]. Because the ground truth data comes from an invariant base, the \mathcal{I} -PANN model outperforms the λ -PANNs during training. Nevertheless, both models achieve excellent losses on the order of 10^{-5} . Interestingly, in the extrapolation

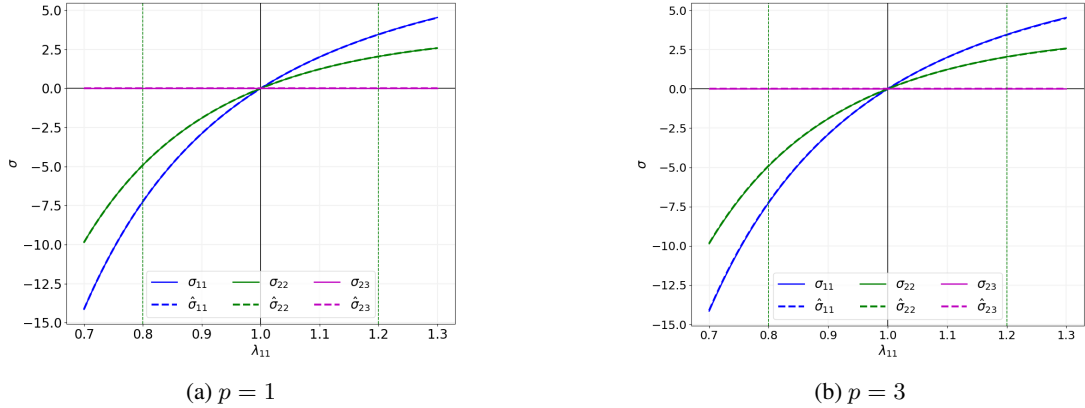


Figure 4: Visualizing response of λ -PANNs on Dataset 5 of λ -Ogden set. Dotted green lines indicate the training domain of 20%. Dashed lines denote model predictions and solid lines denote ground truth response.

Table 3: Generalized Ogden parameters

c_{10}	c_{20}	c_{30}	c_{01}	c_{02}	c_{03}	K
1.583	0.133	-	2.9	0.342	0.248	0.873
1.302	0.261	0.246	0.668	0.245	0.143	0.831
0.875	0.181	-	1.433	0.312	0.229	0.804
0.786	0.577	-	1.268	1.334	-	0.86
1.221	0.126	-	2.874	0.228	-	0.493
0.909	0.318	0.18	2.604	0.238	-	0.743
2.892	0.248	-	0.869	0.312	0.246	0.931
0.567	0.533	0.408	0.253	0.236	-	0.954
0.967	0.906	0.241	0.341	0.185	-	0.968
2.234	0.13	-	2.762	0.109	-	0.391

dataset, with deformations in which the maximum principal stretch exceeds 1.2, the λ -PANNs with $p = 2, 3$ show notably lower losses compared to the \mathcal{I} -PANN model. None of the models show signs of over-fitting.

Having established the ability of the proposed λ -PANN architecture to capture stress-strain data synthetically generated with the Ogden model or the generalized invariant model, we further evaluated the effect of hyperparameter tuning and ablation of the various architecture components. The exponent in the p -norm evaluation at the center of the permutation-invariant neural network was already evaluated in Figs. 3 and 5, which showed that $p = 3$ had the best performance in both training and validation datasets.

Fig. 6 shows the effect of nesting multiple permutation invariant and input-convex neural networks. The more general framework illustrated in Fig. 2 consists of two permutation invariant neural networks, one for capturing convex functions of \mathbf{U} and one for capturing convex functions of $\text{cof}\mathbf{U}$. These permutation invariant neural networks are based on Hölder’s power deep sets Eq. (18) in which an ICNN ϕ is nested within another ICNN ρ which is also non-decreasing. Thus, one of the ablation studies we performed was to disregard the ϕ network but otherwise keep the rest of the architecture. The λ -PANN with no ϕ network has a much slower convergence than the original λ -PANN, as seen in Fig. 6a. Nevertheless, after 100k epochs, the loss in the λ -PANN with no ϕ network approaches values seen in the original λ -PANN. Similar trends can be seen in the validation loss, Fig. 6b. Thus, the ϕ network in Eq. (18) provides flexibility to the architecture that helps it attain lower training and validation losses.

A second ablation study explored the relevance of the last ICNN, $\psi^{NN}(\psi_F, \psi_{\text{cof}F}, J, -2J)$, which takes in as inputs the outputs of the permutation invariant networks ψ_F and $\psi_{\text{cof}F}$. We tested whether such nonlinear nesting would be required for performance. Thus, as an alternative, we tested an additive framework of the form $\psi_F + \psi_{\text{cof}F} + \psi_J(J)$ for which ψ_J is an ICNN which is just a function of J . The performance of this additive strain energy function is shown in Fig. 6. Both training and validation losses of the additive neural network are significantly worse than the proposed λ -PANN which includes the nonlinear nesting $\psi^{NN}(\psi_F, \psi_{\text{cof}F}, J, -2J)$.

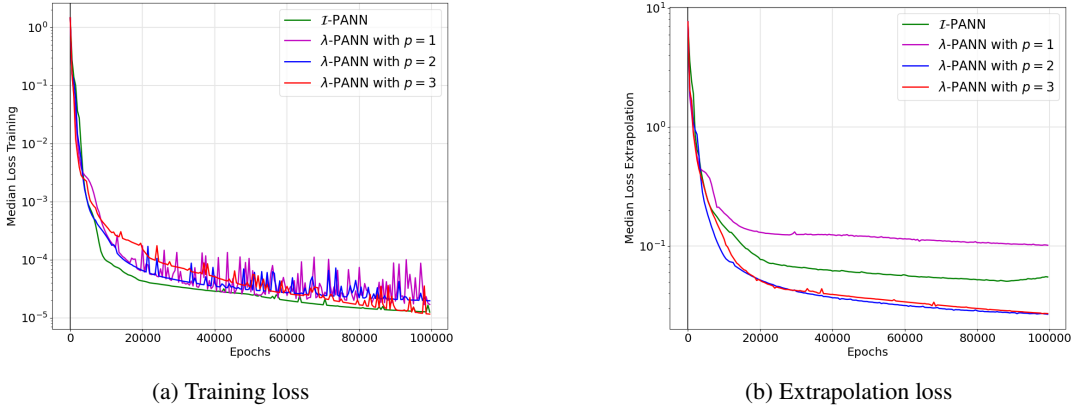


Figure 5: Generalized Ogden model median losses over 10 random models as specified in Table 3. a) Training loss; b) Extrapolation loss.

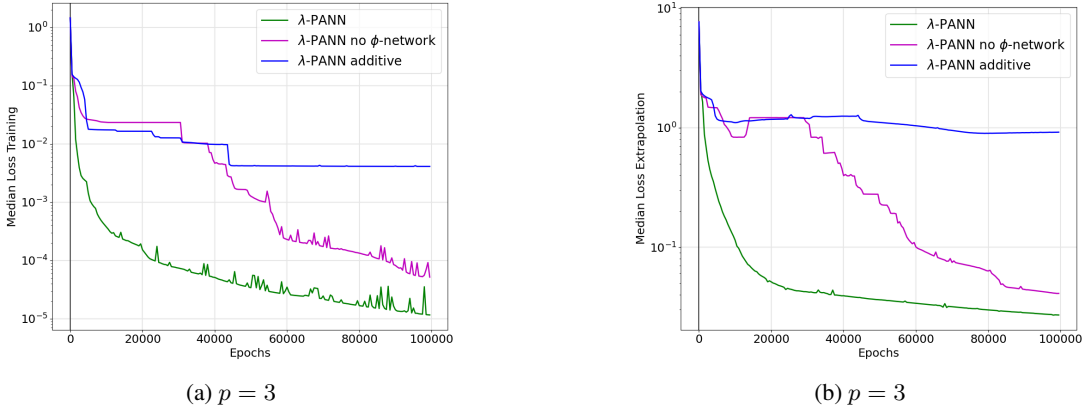


Figure 6: Influence of network architecture for $p = 3$ for the Generalized Ogden data

The last hyperparameter tuning we investigated was to vary the number of parameters by changing the number of layers to $\{1, 2, 3, 4\}$. As seen in Fig. 7, when each of the neural networks of the λ -PANN has only one layer, the training loss is the minimum, but the extrapolation loss is at its maximum. Four layers seems to be optimal for the cases considered. However, all four cases had satisfactory training losses $\leq 10^{-4}$ and extrapolation losses $\leq 10^0$.

We used the optimal λ -PANN architecture identified with the synthetic datasets and applied it to the experimental rubber datasets from Treloar [45] and Heulliet [46]. To regularize our networks and prevent overfitting due to the limited number of experimental data points, we have used L^0 -regularization, see [47, 10]. We have used the same hyperparameters for this regularization as in our previous work [48] and a regularization factor of 10^{-4} between the data loss and the L^0 -loss term.

These datasets contain stress-strain curves under uniaxial tension (UT), pure shear (PS), and equibiaxial tension (ET). We use the UT and ET data to train the model and the PS data to validate its ability to generalize. The λ -PANN accurately captured the experimental data, with a loss on the order of $\sim 10^0$ and $\sim 10^{-1}$ for the Treloar and Heulliet datasets respectively (Figs. 8b and 8d). The number of active parameters in the final network is shown in blue. These are reduced due to L^0 -regularization.

As a further indication of the accurate fit, we report R^2 values of the fits in Figs. 8a and 8c. In all cases $R^2 > 0.99$, highlighting that the trained constitutive model is also able to generalize well to unseen deformation modes (PS case).

5.1 Finite element analysis

We implemented the λ -PANN architecture ($p = 3$) trained on the first parameter set of the Ogden model (see Table 3) into the open source finite element package *Florence* [49]. Fig. 9 shows the benchmark boundary value problem known as Cook’s membrane, which we chose to test our implementation of the λ -PANN model.

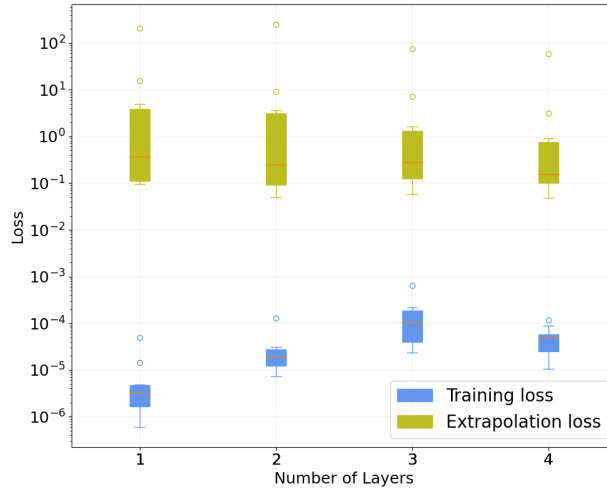


Figure 7: Impact of increasing the network size of λ -PANNs for $p = 3$ for the Ogden dataset described in Table 2. Each of the three subnetworks has 20 neurons per layer where the number of layers sees an increase from 1 to 4.

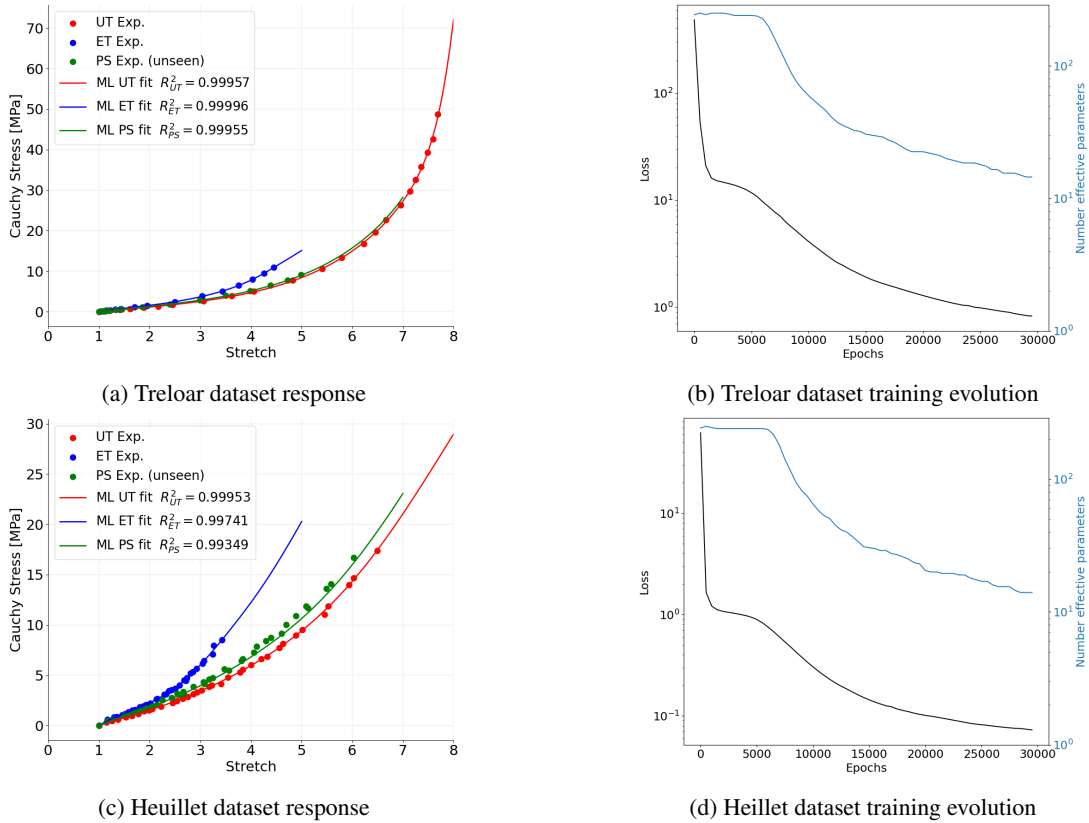


Figure 8: Applying λ -PANNs ($p = 3$) on experimental rubber data. (a,b) Treloar data set [45] stress response and loss and parameter evolution over training iterations, (c,d) Heuillet data set [46] stress response and loss and parameter evolution over training iterations

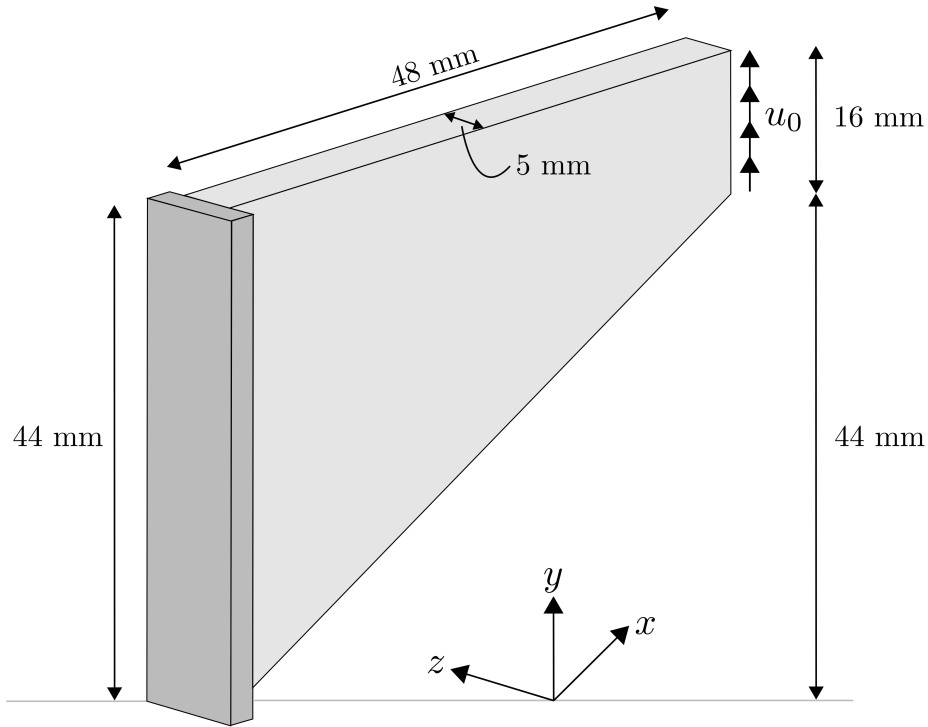


Figure 9: Structural Cook's membrane benchmark.

Fig. 10 shows side by side the stress contour prediction for the Cook's membrane problem using either the closed-form Ogden model Eq. (10) or the λ -PANN architecture. Fig. 11 further shows an accuracy plot between the stresses σ_{xx} obtained from either the closed-form Ogden model or the λ -PANN model trained on the Ogden data. With $R^2 = 0.999$ it is clear that the implementation into the finite element package is correct.

6 Discussion

In this manuscript, we present a physics-augmented data-driven constitutive model framework for hyperelastic materials in terms of principal stretches. By working with the eigenvalues of the right stretch tensor \mathbf{U} , the framework can satisfy objectivity. To satisfy polyconvexity, a sufficient condition for the existence of minimizers of the strain energy in boundary value problems (pending some growth conditions on the strain energy), the framework relies on the nesting of input-convex functions of \mathbf{U} , its cofactor $\text{cof}\mathbf{U}$, and its determinant $\det \mathbf{U}$. To guarantee isotropy and objectivity, we rely on permutation-invariant neural networks known as Holder deep power sets. In particular, we embed input-convex neural networks into the deep-set formulation, yielding symmetric convex functions of the eigenvalues of \mathbf{U} , and of its cofactor $\text{cof}\mathbf{U}$. The framework accurately captures synthetic and experimental data, both within and outside of the training range of deformations. The framework can be readily implemented into finite element packages such as *Jax-FEM* [50] or *Florence*, as we do here [49].

In recent years, numerous data-driven constitutive models have been proposed, primarily formulated in terms of the invariants of the right Cauchy-Green deformation tensor, \mathbf{C} . Notable exceptions include the constitutive artificial neural networks by St. Pierre et al. [17] and the automated model discovery framework EUCLID [14]. However, these approaches extend the Ogden model by expressing the strain energy as a linear combination of multiple Ogden terms [16, 19], rather than providing a truly general material representation in terms of principal stretches. While such an Ogden-like expansion can describe a broad class of materials, it remains a specialized form and may fail in certain cases [51]. Furthermore, the commonly used expansions, Eq. (9), completely disregard the dependence on $\text{cof}\mathbf{F}$.

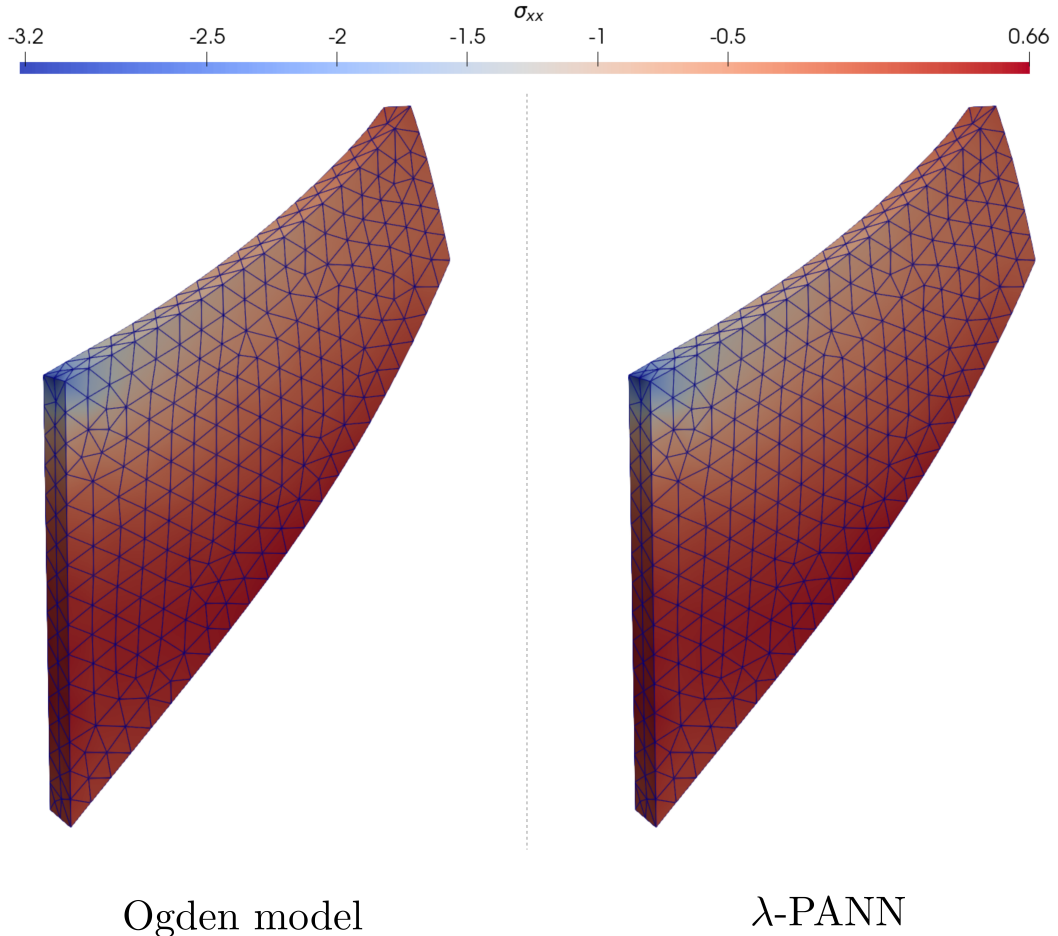


Figure 10: σ_{xx} in the Cook's membrane model for the ground truth Ogden model (left) and the trained λ -PANN (right).

Interestingly, the general Ogden material [21, 22], includes both contributions from \mathbf{C} and $\text{Adj}\mathbf{C}$ (closely related to $\text{cof}\mathbf{F}$),

$$\Psi(\mathbf{F}) = \sum_{i=1}^m a_i \text{tr}(\mathbf{C}^{a_i/2}) + \sum_{j=1}^n b_j \text{tr}((\text{Adj}\mathbf{C})^{b_j/2}) + \Gamma(\det \mathbf{F}), \quad (23)$$

with

$$\begin{aligned} \text{tr}(\mathbf{C}^{a/2}) &= \lambda_1^a + \lambda_2^a + \lambda_3^a \\ \text{tr}((\text{Adj}\mathbf{C})^{b/2}) &= (\lambda_1\lambda_2)^b + (\lambda_1\lambda_3)^b + (\lambda_2\lambda_3)^b. \end{aligned} \quad (24)$$

However, this general expression is almost never used by practitioners. Our additive expansion, explored in Fig. 6, is closely related to Eq. (23), but instead of powers of the eigenvalues of \mathbf{U} and $\text{cof}\mathbf{U}$ we employ the more general ICNN functions $\psi_{\mathbf{F}}, \psi_{\text{cof}\mathbf{F}}$. The results in Fig. 6 show that this additive decomposition is still limiting because it is unable to capture other nonlinear coupling terms. A fully nested structure was necessary to obtain a general functional form with excellent performance across all cases (see Fig. 6).

Invariant-based data-driven models have proven effective in representing a wide range of materials. However, it remained unexplored whether similarly flexible formulations could be formulated in terms of principal stretches. By capturing arbitrary convex symmetric functions with the convolution of deep Holder sets and ICNNs, it is unsurprising that the λ -PANN model performs comparably to the invariant-based \mathcal{I} -PANN when tested against synthetic and

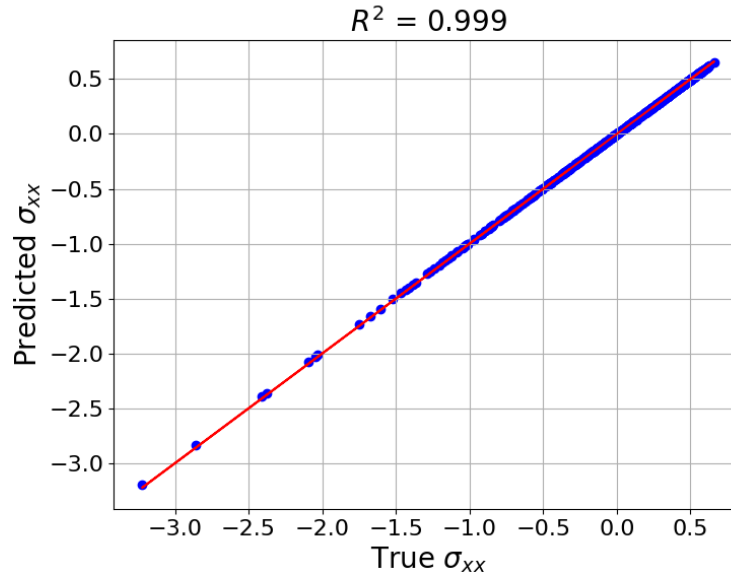


Figure 11: R^2 between true σ_{xx} coming from the ground truth Ogden model and the predicted σ_{xx} obtained by using the trained λ -PANN over all nodes of the Cook’s membrane problem.

experimental data. Notably, λ -PANNs matched the performance of \mathcal{I} -PANN even when trained on data generated from an invariant-based model. However, when the data originated from an Ogden model, λ -PANNs outperformed the \mathcal{I} -PANN, particularly in extrapolation tasks. The λ -PANN architecture also captured the experimental data with high accuracy and generalized well to unseen loading modes. This suggests that while both frameworks are highly flexible and capable of capturing complex material behavior, λ -PANNs may offer a slight advantage

The performance of the λ -PANN was sensitive to the choice of hyperparameters. As mentioned above, the additive structure was unable to capture the synthetic examples, and a fully nested architecture was needed. For the fully nested λ -PANN, performance was influenced by the deep power set exponent $p = 1, 2, 3$ and whether the p -norm operated on the convex function ϕ . Our results indicate that $p = 3$ with ϕ led to the best performance, achieving faster convergence compared to cases without ϕ and lower p . This raises the question of whether even larger values of p could further improve performance. As p increases, the formulation approaches the *max* norm, which is somewhat counterintuitive as it suggests that emphasizing the largest eigenvalue could yield the best constitutive model, but this remains to be tested.

While a fully nonlinear architecture was required, this did not imply an excessively large number of parameters. The intrinsic dimensionality of the data is relatively low. This is clear in synthetic data cases where the ground truth is represented with a small number of parameters, but it is expected in the experimental data cases as well [10, 13]. In the synthetic cases, Fig. 2 shows that even using a single layer in each of $\psi_{\mathbf{F}}, \psi_{\text{cof}\mathbf{F}}, \psi^{NN}$ achieves a low loss. This is likely related to the nonlinear nesting of functions in the architecture. In the experimental case, for which we used the architecture with two layers in each neural network, we applied L_0 regularization to enforce sparsity [10], reducing the number of parameters to approximately 10^1 . Thus, while fully nonlinear nesting is essential, achieving strong performance with a relatively small number of parameters is still possible.

We implemented the λ -PANN model into a finite element package. However, caution is required when computing the tangent stiffness, as it involves derivatives of the eigenvectors, which may not be uniquely defined when eigenvalues are repeated. This challenge is inherent not only to data-driven models but also to analytical models in terms of the principal stretches. Nevertheless, our finite element implementation showed no issues due to the usage of automatic differentiation on the strain energy function evaluated on numerically perturbed eigenvalues.

This work is not without limitations. One limitation is the restriction to isotropic functions, whereas many soft materials, including biological tissues, exhibit anisotropy. Invariant-based models offer a natural advantage in this regard, as pseudo-invariants that account for material symmetries can be readily identified. Moving forward, an important direction would be to establish a corresponding set of *invariants* in terms of eigenvalues and structural tensors. Even within the isotropic setting, however, the present formulation represents the most general principal-stretch-based model, go-

ing even beyond the general Ogden expansion Eq. (23), which has remained the most common principal-stretch model for over fifty years. We anticipate that this work will stimulate further exploration of eigenvalue-based constitutive models, expand the use of data-driven strain energy functions, and lead to extensions accounting for dissipative mechanisms such as damage and viscoelasticity.

7 Conclusion

In this study, we introduced a physics-augmented, data-driven constitutive model framework for hyperelastic materials formulated in terms of principal stretches. By leveraging input-convex and permutation-invariant neural networks, we ensured polyconvexity, objectivity, and isotropy in our proposed λ -PANN architecture. Our model demonstrated strong performance across synthetic and experimental datasets, accurately capturing stress-strain relationships while generalizing well to unseen deformation modes. Notably, λ -PANNs outperformed invariant-based neural network models in extrapolation tasks, particularly when trained on Ogden-generated data.

Our finite element implementation further validated the efficacy of the λ -PANN model, yielding stress predictions nearly identical to those of the ground truth Ogden model in the Cook’s membrane benchmark. This highlights the practical applicability of the proposed architecture in real-world computational mechanics problems.

Ultimately, this study advances the use of polyconvex, data-driven approaches in computational mechanics, providing a flexible and physically consistent alternative to existing invariant-based formulations. We anticipate that this work will inspire further research into eigenvalue-based constitutive models, enhancing our ability to model complex material behavior with data-driven methods.

Data and Code

After the acceptance of this manuscript the code and data will be made available under <https://github.com/FuhgJan/polyConvexPrincipalStrain>.

References

- [1] Hanxun Jin, Enrui Zhang, and Horacio D Espinosa. Recent advances and applications of machine learning in experimental solid mechanics: A review. *Applied Mechanics Reviews*, 75(6):061001, 2023.
- [2] Jan N Fuhg, Govinda Anantha Padmanabha, Nikolaos Bouklas, Bahador Bahmani, WaiChing Sun, Nikolaos N Vlassis, Moritz Flaschel, Pietro Carrara, and Laura De Lorenzis. A review on data-driven constitutive laws for solids. *Archives of Computational Methods in Engineering*, pages 1–43, 2024.
- [3] Vahidullah Taç, Kevin Linka, Francisco Sahli-Costabal, Ellen Kuhl, and Adrian Buganza Tepole. Benchmarking physics-informed frameworks for data-driven hyperelasticity. *Computational mechanics*, 73(1):49–65, 2024.
- [4] Jamshid Ghaboussi and Djonni Eka Sidarta. New nested adaptive neural networks (nann) for constitutive modeling. *Computers and Geotechnics*, 22(1):29–52, 1998.
- [5] Trenton Kirchdoerfer and Michael Ortiz. Data-driven computational mechanics. *Computer Methods in Applied Mechanics and Engineering*, 304:81–101, 2016.
- [6] Yousef Heider, Kun Wang, and WaiChing Sun. So (3)-invariance of informed-graph-based deep neural network for anisotropic elastoplastic materials. *Computer Methods in Applied Mechanics and Engineering*, 363:112875, 2020.
- [7] Kailai Xu, Daniel Z Huang, and Eric Darve. Learning constitutive relations using symmetric positive definite neural networks. *Journal of Computational Physics*, 428:110072, 2021.
- [8] Arif Hussain, Amir Hosein Sakhaei, and Mahmood Shafiee. Machine learning-based constitutive modelling for material non-linearity: A review. *Mechanics of Advanced Materials and Structures*, pages 1–19, 2024.
- [9] Faisal As’ad, Philip Avery, and Charbel Farhat. A mechanics-informed artificial neural network approach in data-driven constitutive modeling. *International Journal for Numerical Methods in Engineering*, 123(12):2738–2759, 2022.
- [10] Jan Niklas Fuhg, Reese Edward Jones, and Nikolaos Bouklas. Extreme sparsification of physics-augmented neural networks for interpretable model discovery in mechanics. *Computer Methods in Applied Mechanics and Engineering*, 426:116973, 2024.

- [11] Vahidullah Taç, Francisco Sahli Costabal, and Adrian B Tepole. Data-driven tissue mechanics with polyconvex neural ordinary differential equations. *Computer Methods in Applied Mechanics and Engineering*, 398:115248, 2022.
- [12] Vahidullah Taç, Manuel K Rausch, Ilias Bilionis, Francisco Sahli Costabal, and Adrian Buganza Tepole. Generative hyperelasticity with physics-informed probabilistic diffusion fields. *Engineering with Computers*, pages 1–19, 2024.
- [13] Kevin Linka, Markus Hillgärtner, Kian P Abdolazizi, Roland C Aydin, Mikhail Itskov, and Christian J Cyron. Constitutive artificial neural networks: A fast and general approach to predictive data-driven constitutive modeling by deep learning. *Journal of Computational Physics*, 429:110010, 2021.
- [14] Moritz Flaschel, Huitian Yu, Nina Reiter, Jan Hinrichsen, Silvia Budday, Paul Steinmann, Siddhant Kumar, and Laura De Lorenzis. Automated discovery of interpretable hyperelastic material models for human brain tissue with euclid. *Journal of the Mechanics and Physics of Solids*, 180:105404, 2023.
- [15] Peiyi Chen and Johann Guilleminot. Polyconvex neural networks for hyperelastic constitutive models: A rectification approach. *Mechanics Research Communications*, 125:103993, 2022.
- [16] Raymond William Ogden. Large deformation isotropic elasticity—on the correlation of theory and experiment for incompressible rubberlike solids. *Proceedings of the Royal Society of London. A. Mathematical and Physical Sciences*, 326(1567):565–584, 1972.
- [17] Sarah R St Pierre, Kevin Linka, and Ellen Kuhl. Principal-stretch-based constitutive neural networks autonomously discover a subclass of ogden models for human brain tissue. *Brain Multiphysics*, 4:100066, 2023.
- [18] Matthew J Lohr, Gabriella P Sugerma, Sotirios Kakaletsis, Emma Lejeune, and Manuel K Rausch. An introduction to the ogden model in biomechanics: benefits, implementation tools and limitations. *Philosophical Transactions of the Royal Society A*, 380(2234):20210365, 2022.
- [19] Michel Destrade, Luis Dorfmann, and Giuseppe Saccomandi. The ogden model of rubber mechanics: 50 years of impact on nonlinear elasticity. *Philosophical Transactions of the Royal Society A*, 380(2234):20210332, 2022.
- [20] Paul Steinmann, Mokarram Hossain, and Gunnar Possart. Hyperelastic models for rubber-like materials: consistent tangent operators and suitability for treloar’s data. *Archive of Applied Mechanics*, 82:1183–1217, 2012.
- [21] H Le Dret. Incompressible limit behaviour of slightly compressible nonlinear elastic materials. *ESAIM: Mathematical Modelling and Numerical Analysis*, 20(2):315–340, 1986.
- [22] Philippe G Ciarlet. *Three-dimensional elasticity*. Elsevier, 1988.
- [23] David J Steigmann. On isotropic, frame-invariant, polyconvex strain-energy functions. *Quarterly Journal of Mechanics and Applied Mathematics*, 56(4):483–491, 2003.
- [24] David Wiedemann and Malte A Peter. Characterization of polyconvex isotropic functions. *arXiv preprint arXiv:2304.08385*, 2023.
- [25] Adrian S Lewis. Convex analysis on the hermitian matrices. *SIAM Journal on Optimization*, 6(1):164–177, 1996.
- [26] Masanari Kimura, Ryotaro Shimizu, Yuki Hirakawa, Ryosuke Goto, and Yuki Saito. On permutation-invariant neural networks. *arXiv preprint arXiv:2403.17410*, 2024.
- [27] Manzil Zaheer, Satwik Kottur, Siamak Ravanbakhsh, Barnabas Poczos, Russ R Salakhutdinov, and Alexander J Smola. Deep sets. *Advances in neural information processing systems*, 30, 2017.
- [28] Gerhard A Holzapfel. *Nonlinear solid mechanics: a continuum approach for engineering science*, 2002.
- [29] Alan N Gent. A new constitutive relation for rubber. *Rubber chemistry and technology*, 69(1):59–61, 1996.
- [30] Hubert M James and Eugene Guth. Theory of the elastic properties of rubber. *The Journal of Chemical Physics*, 11(10):455–481, 1943.
- [31] Ellen M Arruda and Mary C Boyce. A three-dimensional constitutive model for the large stretch behavior of rubber elastic materials. *Journal of the Mechanics and Physics of Solids*, 41(2):389–412, 1993.
- [32] John M Ball. Convexity conditions and existence theorems in nonlinear elasticity. *Archive for rational mechanics and Analysis*, 63:337–403, 1976.
- [33] Matti Schneider. Beyond polyconvexity: an existence result for a class of quasiconvex hyperelastic materials. *Mathematical Methods in the Applied Sciences*, 40(6):2084–2089, 2017.
- [34] Stephen Boyd and Lieven Vandenberghe. *Convex optimization*. Cambridge university press, 2004.

- [35] Ch Miehe. Aspects of the formulation and finite element implementation of large strain isotropic elasticity. *International journal for numerical methods in engineering*, 37(12):1981–2004, 1994.
- [36] Hüsnü Dal, Funda Aksu Denli, Alp Kağan Açı, and Michael Kaliske. Data-driven hyperelasticity, part i: A canonical isotropic formulation for rubberlike materials. *Journal of the Mechanics and Physics of Solids*, 179:105381, 2023.
- [37] Phoebus Rosakis. Characterization of convex isotropic functions. *Journal of elasticity*, 49:257–267, 1997.
- [38] Stefan Hartmann and Patrizio Neff. Polyconvexity of generalized polynomial-type hyperelastic strain energy functions for near-incompressibility. *International journal of solids and structures*, 40(11):2767–2791, 2003.
- [39] Lennart Linden, Dominik K Klein, Karl A Kalina, Jörg Brummund, Oliver Weeger, and Markus Kästner. Neural networks meet hyperelasticity: A guide to enforcing physics. *Journal of the Mechanics and Physics of Solids*, 179:105363, 2023.
- [40] Jan N Fuhg and Nikolaos Bouklas. On physics-informed data-driven isotropic and anisotropic constitutive models through probabilistic machine learning and space-filling sampling. *Computer Methods in Applied Mechanics and Engineering*, 394:114915, 2022.
- [41] Diederik P Kingma. Adam: A method for stochastic optimization. *arXiv preprint arXiv:1412.6980*, 2014.
- [42] Asghar A Jadoon, Karl A Kalina, Manuel K Rausch, Reese Jones, and Jan N Fuhg. Inverse design of anisotropic microstructures using physics-augmented neural networks. *arXiv preprint arXiv:2412.13370*, 2024.
- [43] Dominik K Klein, Mauricio Fernández, Robert J Martin, Patrizio Neff, and Oliver Weeger. Polyconvex anisotropic hyperelasticity with neural networks. *Journal of the Mechanics and Physics of Solids*, 159:104703, 2022.
- [44] Jan N Fuhg, Nikolaos Bouklas, and Reese E Jones. Learning hyperelastic anisotropy from data via a tensor basis neural network. *Journal of the Mechanics and Physics of Solids*, 168:105022, 2022.
- [45] Leslie RG Treloar. Stress-strain data for vulcanized rubber under various types of deformation. *Rubber Chemistry and Technology*, 17(4):813–825, 1944.
- [46] P Heuillet and L Dugautier. Modélisation du comportement hyperélastique des caoutchoucs et élastomères thermoplastiques, compacts ou cellulaires. *Génie mécanique des caoutchoucs et des élastomères thermoplastiques*, 1997.
- [47] Christos Louizos, Max Welling, and Diederik P Kingma. Learning sparse neural networks through l_0 regularization. *arXiv preprint arXiv:1712.01312*, 2017.
- [48] Jan N. Fuhg, Asghar Jadoon, Oliver Weeger, D. Thomas Seidl, and Reese E. Jones. Polyconvex neural network models of thermoelasticity. *Journal of the Mechanics and Physics of Solids*, 192:105837, 2024.
- [49] florence. <https://github.com/romeric/florence>, 2025.
- [50] Tianju Xue, Shuheng Liao, Zhengtao Gan, Chanwook Park, Xiaoyu Xie, Wing Kam Liu, and Jian Cao. Jax-fem: A differentiable gpu-accelerated 3d finite element solver for automatic inverse design and mechanistic data science. *Computer Physics Communications*, page 108802, 2023.
- [51] Afshin Anssari-Benam, Michel Destrade, and Giuseppe Saccomandi. Modelling brain tissue elasticity with the ogden model and an alternative family of constitutive models. *Philosophical Transactions of the Royal Society A*, 380(2234):20210325, 2022.